

Enhanced terahertz wave emission from air-plasma tailored by abruptly autofocusing laser beams

KANG LIU,¹ ANASTASIOS D. KOULOUKLIDIS,^{2,3} DIMITRIOS G. PAPAZOGLU,^{2,3}
STELIOS TZORTZAKIS,^{2,3,4} AND XI-CHENG ZHANG^{1,*}

¹The Institute of Optics, University of Rochester, 275 Hutchison Road, Rochester, New York 14627, USA

²Institute of Electronic Structure and Laser, Foundation for Research and Technology-Hellas, P.O. Box 1527, 71110 Heraklion, Greece

³Department of Material Science and Technology, University of Crete, P.O. Box 2208, 71003 Heraklion, Greece

⁴Science Program, Texas A&M University at Qatar, P.O. Box 23874, Doha, Qatar

*Corresponding author: xi-cheng.zhang@rochester.edu

Received 10 February 2016; revised 2 May 2016; accepted 13 May 2016 (Doc. ID 259260); published 6 June 2016

Developing coherent intense broadband light sources is undoubtedly one of the key elements in pushing the frontiers of optical sciences, especially those of nonlinear terahertz (THz) optics. Plasma-based THz emitters excel in many aspects thanks to their broad radiation bandwidth, high output pulse energy and immunity to high power damage. Various excitation wavelengths and gases have been explored in the search for a stronger THz wave emission from laser-induced plasmas, whereas few attempts have been made with artificially modulated exotic wavepackets. Here we demonstrate that abruptly autofocusing-beam-induced air-plasma can give a 5.3-times enhanced THz wave pulse energy compared to normal Gaussian-beam-induced plasma under the same conditions. We believe this work will inspire a new direction for controlling THz radiation from laser-induced plasma using tools such as spatial light modulators to sculpt the excitation beams, and pave the way to THz remote spectroscopy, which is considered critical for both homeland security and environmental monitoring. © 2016 Optical Society of America

OCIS codes: (350.5400) Plasmas; (350.5500) Propagation; (190.4380) Nonlinear optics, four-wave mixing; (300.6495) Spectroscopy, terahertz.

<http://dx.doi.org/10.1364/OPTICA.3.000605>

Since the first demonstrations of 1D and 2D accelerating Airy beams [1,2], studies on the family of abruptly autofocusing (AAF) beams started to draw much attention in the nonlinear optics community. Shortly after the prediction of the radially symmetric Airy beam (ring Airy) in 2010 [3], its unusual properties, such as the ability to autofocus with a parabolic trajectory and to abruptly increase the maximum intensity at the focus by orders of magnitude, were experimentally observed [4]. At the same time, a new family of $(2 + 1)$ D AAF beams with pre-engineered arbitrary focusing caustics was introduced by Chremmos *et al.* [5]. A wide range of possible applications, such as medical laser

treatment, microparticle trapping, and temporal cloaking, were discussed in numerous reports [5–7].

The nonlinear propagations of novel beams other than Gaussian is always an area of interest for filamentation researchers [8–10]. The use of these beams not only helps design the spatial profile of the plasma, but also enables various broadband radiations from the plasma, such as supercontinuum radiation [11] or terahertz (THz) radiation [12], giving hope to multiple remote-spectroscopy applications [13]. For the AAF beams, the nonlinear propagations were already observed in fused silica [14], but experimental results in air have yet to be demonstrated.

One of the many promising applications of air-plasma is to serve as an intense broadband tabletop THz source. Single-color plasma was first reported to generate THz radiation by Hamster *et al.* [15]. Later, it was proved to be several orders of magnitudes more efficient if two-color (fundamental and the second harmonic) plasma is used [16]. Using different plasma parameters to improve generation efficiency is a new area of interest for numerous research groups [17,18]. Among those efforts, some have tried tailoring the plasma in different ways, such as creating plasma with gradient distribution [19], concatenating two plasmas into one [20], and putting two filaments side by side [21]. They have found that, with those methods, they can achieve either enhancement or control of the THz radiation from the tailored two-color air-plasmas.

In this work, we investigate the characteristics of THz radiation from two-color AAF-beam-induced air-plasma. AAF beams' high level of tenability [5], wavepacket stability in the nonlinear regime [14], and robustness when propagating in turbulent media [22] make plasmas induced by these novel wavepackets a promising broadband THz source for THz remote sensing and spectroscopy [13,23], a critical topic for homeland security and environmental monitoring. The AAF beams used in this work were pre-engineered to have the same autofocusing curve as the familiar parabolic trajectory of ring-Airy beams [5].

The measurements exploited a pump-probe THz time-resolved detection system, shown in Fig. 1(a). The AAF beams were generated by sending 35 fs, 50 Hz, 800 nm Ti:sapphire laser pulses to a spatial light modulator (SLM, Hamamatsu

LCOS-X10468-2), with a phase mask exerted. Following an approach similar to that of Chremmos *et al.* [5], the phase mask consisted of a radially chirped phase distribution $\varphi(r) = C \cdot (r - r_0)^{3/2}$, $\forall r \geq r_0$ and $\varphi(r) = 0$, $\forall r < r_0$, where r is the radius, r_0 is a reference radius, and C is a constant. By blocking the central part of the phase-modulated Gaussian beam with an opaque disk, after some free propagation, a ring-Airy distribution was formed [5]. This method is energetically advantageous compared to a Fourier transform approach [4], since the loss of a large amount of energy in the zero-order was avoided. The Gaussian beams were generated by sending the same laser pulses to the SLM with a plain phase mask. When using the Gaussian beam, the opaque disk was removed from the beam path, as shown in the zoom-in parts of Fig. 1(a).

The experimental setup was designed to compare the THz radiation from air-plasmas induced by AAF beams and Gaussian beams. To increase the intensity enough to generate plasma in air and to precisely position the plasma, in both cases the pump beam was focused by a 100 mm focal length lens, as shown in Fig. 1(a). The focused AAF pump beam preserves the AAF properties, such as the abrupt focusing, except that now the focus is more intense and is shifted toward the laser source. A 50- μm -thick β -barium borate (BBO) was put between the lens and the plasma to create the second-harmonic (SH) generation of the pump pulse. The SH of the AAF beam retains its abrupt autofocusing characteristic, sharing the same acceleration as the fundamental harmonic (FH) [24]. Interestingly, the abrupt autofocusing foci of the fundamental AAF and its SH overlap in space. Detailed descriptions of the lens-focused AAF beam and the properties of its SHs are

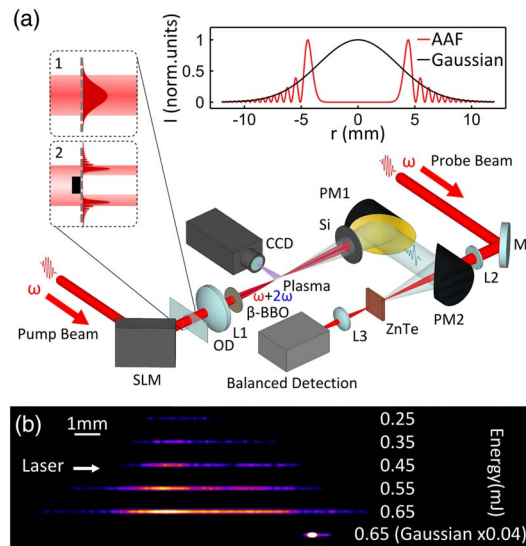


Fig. 1. (a) Experimental setup: SLM, spatial light modulator; OD, opaque disk, onto a transparent glass slide; L, lens; PM, parabolic mirror; M, mirror. Inset, top right: schematic comparison between the radial intensity distribution of the AAF and the Gaussian beam. Inset, top left: zoom-in on the beam area before and after the glass slide. Case 1 uses the Gaussian beam; the glass slide is shifted so the OD is removed from the beam path. Case 2 uses the AAF beam; the OD is moved back into the center of the beam to block the unwanted part. (b) Fluorescence false color images of AAF beam plasmas (top 5) with pulse energy from 0.25 to 0.65 mJ, and Gaussian beam plasma (bottom) with pulse energy 0.65 mJ. The Gaussian plasma image intensity has been reduced 25 times to reach similar visibility of the AAF beam plasmas.

out of the scope of this Letter and will be addressed in separate publications [25,26]. The pulse energy of the pump beam before the β -BBO ranged from 0.1 to 0.65 mJ. The maximum energy that could be applied was limited by the onset of white-light generation in the lens that would cause damage.

Free-space electro-optic sampling with a 3-mm-thick (110) cut ZnTe was used to detect THz waveforms [27]. A pair of off-axis-parabolic-mirrors was used to collect, collimate, and re-focus the forward THz radiation from the plasma. Fluorescence images of the generated plasmas were recorded using a linear CCD camera and imaging optics.

The fluorescence distribution emission $F(r, z)$ for various input optical energies is shown in Fig. 1(b). In the figure, from top to bottom, the plasma images are respectively formed by focusing AAF beams with 0.25, 0.35, 0.45, 0.55, and 0.65 mJ pulse energy. It is clearly observed that the peak intensity of the plasma string shifts as the input energy increases. Also observable is the emergence of low-intensity secondary peaks following the primary focus, as a characteristic feature of ring-Airy beams. At high energy, the secondary peaks are merged with the main peak to a single plasma string. These nonlinear propagation phenomena in air agree very well with the nonlinear propagation of ring-Airy beams in the bulk of fused silica reported in 2013 by Panagiotopoulos *et al.* [14]. When we compare the plasmas induced by AAF and Gaussian beams [bottom trace in Fig. 1(b)], we notice that the AAF beam induced plasma is significantly longer in contrast to the Gaussian plasma. Not only the length difference is apparent, but the difference in fluorescence emission intensity is also obvious. For example, with 0.65 mJ pump pulse energy, the maximum recorded fluorescence intensity of the Gaussian plasma is 210 times brighter than that of plasma generated by the AAF beam.

Figures 2(a) and 2(b) show the THz waveform and its spectrum generated by an AAF-beam-induced plasma. The signal

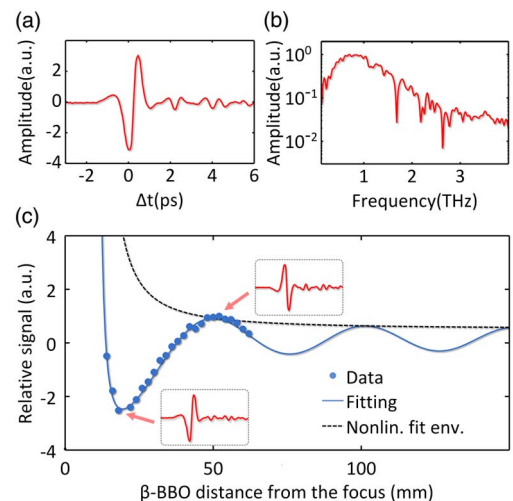


Fig. 2. (a) Typical THz waveform generated from the AAF-beam-induced plasma pumped with a pulse energy of 0.65 mJ. (b) The corresponding spectrum. (c) THz emission peak amplitude versus the β -BBO distance from the focus: blue dots, experimental data; blue solid curve, FWM model fitting result; black dashed curve, nonlinear fitting envelope taking into account the SH generation efficiency change as the β -BBO is moving toward the focus. The insets show two sample THz waveforms having opposite polarities.

was optimized through tuning the relative phase and intensity proportion between the FH (800 nm) and the SH (400 nm) by adjusting the position and angle of the β -BBO crystal. The spectral bandwidth of the detected THz signal is essentially limited by the phonon absorption of the ZnTe crystal.

Because the AAF air-plasma THz source under study shares the same asymmetrical laser field and interaction material with the familiar Gaussian air-plasma THz source, a THz emission process similar to that of a Gaussian source is expected. To confirm this expectation, we measured the THz peak amplitude as a function of the relative phase between the two colors by scanning the β -BBO between the focus and the lens. The scanning range of the crystal was limited by the focal length of the lens and the damage threshold of the BBO. The results are shown in Fig. 2(c). The THz yield modulation is due to the variation of the relative phase between the two colors. The insets give examples of how the relative phase controls the THz radiation waveform polarity. Also shown in Fig. 2(c) is that these data can be fitted with the four-wave-mixing (FWM) model [28] while taking into account how the SH generation efficiency would change as the β -BBO crystal moves closer to the plasma due to the beam intensity change on the crystal. The resulting fitting parameters give a THz yield modulation oscillation period that is consistent with the known dispersion in air [29].

Figure 3 shows the emitted THz amplitude as a function of the input pulse energy. The red dots are the experimental data from the AAF beam plasma, which can be fitted with the FWM model: $E_{\text{THz}} \propto a\chi^{(3)}I(I - bI^2)$ [28], where E_{THz} is the emitted THz field amplitude, a and b are constants, I is the total beam intensity before the BBO crystal, and $\chi^{(3)}$ is the third-order susceptibility of air. The fitting result shows that the experimental data starts to deviate from the fitting curve at around 0.45 mJ and the deviation becomes prominent at 0.55 mJ. This implies that, for higher pulse energies, one should consider the photocurrent model and the intensity clamping in the filaments [30,31]. There could also be contribution from the nonlinear interaction between the beam and the lens that can cost some of the energy. When the input pulse energy is high, some energy hot spots observed on the primary ring of the AAF beam tend to cause white-light generation from the lens.

To better characterize the AAF beam plasma as a THz source, we compare its THz emission with the one from a Gaussian-beam-induced plasma under the same experimental conditions.

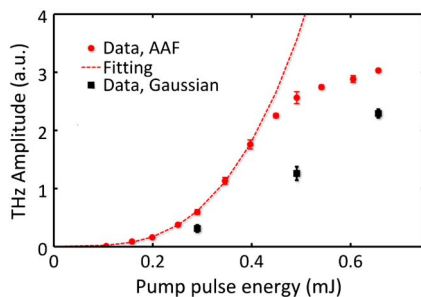


Fig. 3. Emitted THz wave peak amplitude as a function of total pump pulse energy (800 and 400 nm). Red dots, experimental data from the AAF beam; red dashed line, fitting of the AAF data with the FWM model; black squares, data from Gaussian beam under the same initial conditions as a comparison. The error bars show the measurement standard deviation of each point.

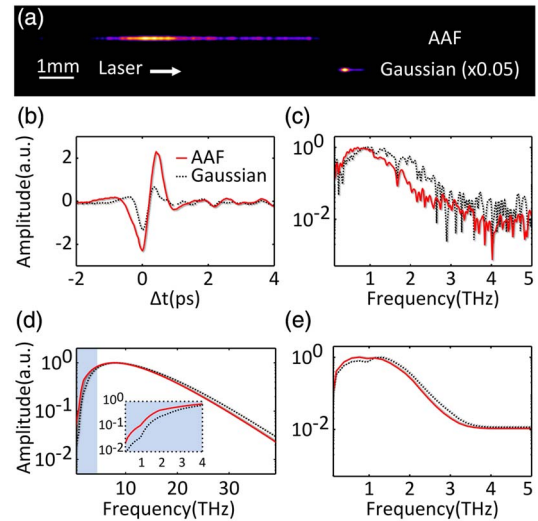


Fig. 4. (a) Fluorescence image comparison between an AAF beam plasma and a Gaussian plasma (intensity reduced by 20 times), both generated with pump pulse energy of 0.5 mJ. (b) Measured THz waveforms and (c) their corresponding normalized spectra generated by the two plasmas in (a). Normalized simulations of THz radiation spectra (d) without and (e) with the 3-mm-thick ZnTe detection bandwidth limitation; the inset in (d) is the enlarged version of the blue area (0–4 THz). Red solid curves, emission from AAF plasma; black dashed curves, emission from Gaussian plasma.

Figure 4(a) shows the images of the plasmas being discussed below. With a 0.5 mJ input pulse energy, the AAF beam plasma THz waveform measured is shown in Fig. 4(b), whereas the one from the Gaussian beam has noticeably lower amplitude. If we calculate the pulse energy by integrating the square of THz field, the THz pulse energy from the AAF plasma is about 5.3 times larger than that from the Gaussian plasma. The obvious THz yield difference can be explained by the significant plasma length difference [32], as we have qualitatively verified with our interference model [33]. Neither plasma has reached the typical air filamentation dephasing length. If we consider the possibility that a shorter plasma may emit THz with a larger angle [33], which means the THz radiation from the Gaussian beam plasma could eventually be focused tighter than that from the AAF plasma, the real THz yield difference between the two might be substantially bigger than what we measured. Figure 4(c) shows the normalized spectra of the waveforms. The AAF plasma THz emission has a central frequency slightly lower than the Gaussian one, which denotes that the AAF plasma has a lower plasma density [29]. A set of power-dependence measurement data of Gaussian beams is also shown in Fig. 3.

During the experiment, the lens location was optimized for each measurement to avoid the signal discrepancy caused by focus location changes. Moreover, a 2-in. (50.8 mm) diameter parabolic mirror with 3-in. (76.2 mm) focal length was put after the plasma to collect the THz radiation, providing an 18.4° collecting angle, sufficient to cover the emission cone ($\sim 10^\circ$) from a two-color air-plasma generated by the 100 mm focal length lens [34].

To validate our hypothesis on the reasons behind the enhanced THz radiation pulse energy of AAF-beam-induced plasma and its redshifted central frequency, we performed simulations using our interference model, which is able to depict the THz

radiation intensity and spectrum of a known plasma [33]. Using the plasma distributions according to the fluorescence images and the numerical estimations of the maximum electron densities for the Gaussian beam ($\sim 10^{17} \text{ cm}^{-3}$) and the AAF beam ($\sim 3 \times 10^{16} \text{ cm}^{-3}$), taking into account the detection bandwidth limitation of a 3-mm-thick ZnTe crystal, the resulting simulated THz radiation pulse energy of an AAF-beam-induced plasma is found to be about 4 times larger than that from the Gaussian plasma source. The normalized calculations of THz radiation spectra from these two THz sources are shown in Fig. 4(e), giving the same type of central frequency difference as experimental measurements display. Both simulation results agree qualitatively well with the measured data. In addition, to predict the THz sources' behavior when using a broadband detection method, such as THz-air-biased-coherent-detection [23] or interferometric detection [29], we also performed a full spectral simulation without the bandwidth limit ZnTe, which indicates that the intensity enhancement and the redshift of the AAF-beam-induced THz radiation would persist regardless of the detection method. Figure 4(d), which shows the normalized full spectrum results with an inset focusing on the low-frequency region, helps to reveal that the AAF-beam-induced THz radiation spectrum would still have a redshift as compared to the Gaussian one. This spectral shift to the low frequency could possibly benefit the THz radiation enhancement of AAF-beam-induced plasma that we measured in the low-frequency region. Even so, considering that 0.1–3 THz is the most commonly used and more advantageous frequency range for THz time-domain spectroscopy [35], the enhancement we achieved through using AAF beam is still exciting.

In conclusion, AAF beams were utilized to generate enhanced THz radiation from their laser-induced air-plasma, in comparison to normal Gaussian beams. We observed that, under the same experimental conditions with 0.5 mJ input pulse energy, the AAF-plasma-generated THz pulse energy is about 5.3 times larger than that from the Gaussian beam, possibly due to the significant plasma length difference. There is a noticeable change in the THz radiation spectrum between the AAF beam and the Gaussian beam that could be attributed to the plasma density difference between the corresponding plasmas. This unique wavepacket-based THz emitter demonstrates the possibility of AAF beam application in THz frequency remote sensing that will enable a high level of control on the excitation beam. It sets a reference for future work involving using different novel wavepackets to tailor the plasma as a THz source. Systematic exploration of the optimum AAF beam parameters for THz generation will possibly entail a further enhancement of THz radiation. Other families of beams may also exhibit interesting physics in regard to THz generation, such as 2D Airy beams [9] or Airy–Airy–Airy light bullets [2]. As more types of novel beam have been reported, using tools like SLMs or phase masks to sculpt the excitation beams could be a new direction for controlling THz radiation from laser-induced plasma.

Funding. U.S. Army Research Office (ARO) (W911NF1110297, W911NF-14-1-0343); "Laserlab-Europe"

(EC-GA 654148); General Secretariat for Research and Technology (GSRT) Aristeia project "FTERA" (2570).

REFERENCES

1. G. A. Siviloglou, J. Broky, A. Dogariu, and D. N. Christodoulides, *Phys. Rev. Lett.* **99**, 213901 (2007).
2. D. Abdollahpour, S. Sunstov, D. G. Papazoglou, and S. Tzortzakis, *Phys. Rev. Lett.* **105**, 253901 (2010).
3. N. K. Efremidis and D. N. Christodoulides, *Opt. Lett.* **35**, 4045 (2010).
4. D. G. Papazoglou, N. K. Efremidis, D. N. Christodoulides, and S. Tzortzakis, *Opt. Lett.* **36**, 1842 (2011).
5. I. Chremmos, N. K. Efremidis, and D. N. Christodoulides, *Opt. Lett.* **36**, 1980 (2011).
6. P. Zhang, J. Prakash, Z. Zhang, M. S. Mills, N. K. Efremidis, D. N. Christodoulides, and Z. Chen, *Opt. Lett.* **36**, 2883 (2011).
7. I. Chremmos, *Opt. Lett.* **39**, 4611 (2014).
8. P. Polynkin, M. Kolesik, A. Roberts, D. Faccio, P. D. Trapani, and J. Moloney, *Opt. Express* **16**, 15733 (2008).
9. P. Polynkin, M. Kolesik, J. V. Moloney, G. A. Siviloglou, and D. N. Christodoulides, *Science* **324**, 229 (2009).
10. M. Scheller, M. S. Mills, M.-A. Miri, W. Cheng, J. V. Moloney, M. Kolesik, P. Polynkin, and D. N. Christodoulides, *Nat. Photonics* **8**, 297 (2014).
11. P. Polynkin, M. Kolesik, and J. Moloney, *Phys. Rev. Lett.* **103**, 123902 (2009).
12. S. Moradi, A. Ganjovi, F. Shojaei, and M. Saeed, *Phys. Plasmas* **22**, 043108 (2015).
13. J. Liu, J. Dai, S. L. Chin, and X.-C. Zhang, *Nat. Photonics* **4**, 627 (2010).
14. P. Panagiotopoulos, D. G. Papazoglou, A. Couairon, and S. Tzortzakis, *Nat. Commun.* **4**, 2622 (2013).
15. H. Hamster, A. Sullivan, S. Gordon, W. White, and R. Falcone, *Phys. Rev. Lett.* **71**, 2725 (1993).
16. D. J. Cook and R. M. Hochstrasser, *Opt. Lett.* **25**, 1210 (2000).
17. X. Xie, J. Dai, and X.-C. Zhang, *Phys. Rev. Lett.* **96**, 075005 (2006).
18. E. Matsubara, M. Nagai, and M. Ashida, *Appl. Phys. Lett.* **101**, 011105 (2012).
19. J. M. Manceau, A. Averchi, F. Bonaretti, D. Faccio, P. Di Trapani, A. Couairon, and S. Tzortzakis, *Opt. Lett.* **34**, 2165 (2009).
20. J. M. Manceau, M. Massaouti, and S. Tzortzakis, *Opt. Lett.* **35**, 2424 (2010).
21. J. Zhao, L. Guo, W. Chu, B. Zeng, H. Gao, Y. Cheng, and W. Liu, *Opt. Lett.* **40**, 3838 (2015).
22. X. Chu, *Opt. Lett.* **36**, 2701 (2011).
23. J. Dai, J. Liu, and X.-C. Zhang, *IEEE J. Sel. Top. Quantum Electron.* **17**, 183 (2011).
24. I. Dolev, I. Kamirer, A. Shapira, M. Segev, and A. Arie, *Phys. Rev. Lett.* **108**, 113903 (2012).
25. A. D. Koulouklidis, D. G. Papazoglou, and S. Tzortzakis, are preparing a manuscript to be called "Abruptly autofocusing harmonic beams."
26. D. G. Papazoglou, V. Y. Fedorov, and S. Tzortzakis, are preparing a manuscript to be called "Conjugate waves focus in a peculiar way."
27. Q. Wu and X. C. Zhang, *Appl. Phys. Lett.* **68**, 1604 (1996).
28. J. Dai and X.-C. Zhang, *Opt. Lett.* **39**, 777 (2014).
29. K. Y. Kim, A. J. Taylor, J. H. Glowina, and G. Rodriguez, *Nat. Photonics* **2**, 605 (2008).
30. H. G. Roskos, M. D. Thomson, M. Kreß, and T. Löffler, *Laser Photon. Rev.* **1**, 349 (2007).
31. T. I. Oh, Y. S. You, N. Jhaji, E. W. Rosenthal, H. M. Milchberg, and K. Y. Kim, *Appl. Phys. Lett.* **102**, 201113 (2013).
32. Y. S. You, T. I. Oh, and K. Y. Kim, *Phys. Rev. Lett.* **109**, 183902 (2012).
33. A. Gorodetsky, A. D. Koulouklidis, M. Massaouti, and S. Tzortzakis, *Phys. Rev. A* **89**, 033838 (2014).
34. V. Blank, M. D. Thomson, and H. G. Roskos, *New J. Phys.* **15**, 075023 (2013).
35. X.-C. Zhang and J. Xu, *Introduction to THz Wave Photonics* (Springer, 2010), p. 52.